



UNITED STATES OF AMERICA  
NUCLEAR REGULATORY COMMISSION

ATOMIC SAFETY AND LICENSING BOARD

In the Matter of

NEXTERA ENERGY SEABROOK, LLC

(Seabrook Station, Unit 1)

Docket No. 50-443-LA-2

ASLBP No. 17-953-02-LA-BD01

Hearing Exhibit

Exhibit Number: NER066

Exhibit Title: Dunant and Scrivener, "Micro-Mechanical Modelling of Alkali-Silica-Reaction-Induced Degradation Using The AMIE Framework," 40 Cement and Concrete Research 4, 517-25 (2010)

See discussions, stats, and author profiles for this publication at: <https://www.researchgate.net/publication/222735277>

# Micro-mechanical modelling of alkali-silica-reaction-induced degradation using the AMIE framework

Article in *Cement and Concrete Research* · April 2010

DOI: 10.1016/j.cemconres.2009.07.024

CITATIONS

80

READS

104

2 authors:



Cyrille F. Dunant

University of Cambridge

47 PUBLICATIONS 2,995 CITATIONS

[SEE PROFILE](#)



Karen L. Scrivener

École Polytechnique Fédérale de Lausanne

307 PUBLICATIONS 12,029 CITATIONS

[SEE PROFILE](#)

Some of the authors of this publication are also working on these related projects:



Innovative engineering approach for material, carbon and cost efficiency of steel buildings [View project](#)



Supply Chain Integration for Structural Steel Reuse - Innovate UK [View project](#)

Micro-mechanical modelling of  
Alkali-Silica–Reaction—Induced Degradation  
Using the Amie Framework

Cyrille F. Dunant, Karen L. Scrivener

October 31, 2008

**Abstract**

Amie, a finite element / extended finite element framework, has been designed to provide the tools to run detailed microstructural simulations; this paper demonstrates the possibility of simulating the mechanisms underlying the alkali-silica–reaction (ASR). The numerical model presented provides a better understanding of experimental observations. Macroscopic free expansion and degradation of mechanical properties have been previously linked to the extent of reaction. The connection between microscopic and macroscopic measurements, simulated by the model, supports the hypothesis that damage is induced by growing gel pockets in the aggregates.

**Keywords:** ASR, XFEM, Damage, Prediction, Modelling

# 13 **1 Introduction**

14 The alkali-silica-reaction (ASR) is characterised by the breakdown of  
15 silanol bonds in poorly crystallised silica found in aggregates in the presence  
16 of alkaline ions. The product of this reaction is an amorphous alkali-silica  
17 “gel” which expands in the presence of moisture, inducing stress in the  
18 microstructure. This causes concrete expansion and mechanical properties  
19 degradation. Prediction of the free expansion, as well as the subsequent  
20 degradation of the stiffness and strength are of great importance for the  
21 owners and managers of affected structures.

22 Mechanical modelling of ASR at the material level poses significant chal-  
23 lenges both technical and scientific. A model based on physics is necessary to  
24 understand the degradation mechanism and to permit prognosis and life-time  
25 assessment of affected structures. Such a model should be based on a detailed  
26 meso-mechanical representation of the concrete microstructure to capture the  
27 variety of mineralogies found in the field.

28 In this paper, we present a micro-mechanical model of ASR implemented  
29 using a purpose-developed extended finite element modelling (XFEM) frame-  
30 work capable of a full scale simulation of laboratory-sized samples in two  
31 dimensions. This framework called AMIE (automated mechanics for inte-  
32 grated experiments) was developed to be very flexible to enable study of  
33 various proposed ASR mechanisms at the meso-structural level[1, 2]. Ben  
34 Haha and colleagues proposed a method to measure the advancement of  
35 the reaction using image analysis to quantify the void and crack content

36 of the aggregates. Macroscopic free expansion was shown to be linked to  
37 this parameter, independent of the curing conditions[3]. We have extended  
38 this study with a wider range of aggregates, and confirmed the relationship  
39 (Fig. 1). The connection between microscopic observations and macroscopic  
40 measurements, simulated by the model, supports the hypothesis that damage  
41 is induced by growing gel pockets in the aggregates.

## 42 **2 ASR models in literature**

43 ASR models are frequently formulated at the material level for use in  
44 structure-level codes, and use empirical relationships[4, 5, 6, 7]. Constructing  
45 models from semi-empirical relations requires extensive experimental cam-  
46 paigns such as in the theses of Poyet[5] and Larive[8], where sufficiently large  
47 datasets are produced which allow robust fitting. The curing conditions, tem-  
48 perature, stress, and relative humidity are varied, and the resulting evolution  
49 of expansion over time is measured as function of those parameters. The  
50 findings from such approaches are extensive and detailed, but are specific to  
51 each aggregate type. Coupling is often introduced between various parameters,  
52 even when these have no direct physical connection, such as aggregate size  
53 and alkali content.

54 Another approach consists in the development of analytical models. Re-  
55 lationships predicting the damage at the material level are derived from  
56 assumptions on the mode of reaction of the aggregates. These models fre-  
57 quently assume gel formation to occur preferentially at the interface between

58 aggregate and paste[9, 10]. The degradation of mechanical properties is  
59 described as coming from the ASR gel which first fills the pores and then  
60 induces expansion and cracks.

61 Numerical models at the level of the microstructure are rare. For example,  
62 such models focus on the fracture mode of a single aggregate such as in the  
63 work of Çopuroğlu and colleagues[11], which computes crack propagation in  
64 a single aggregate using a lattice model.

65 Models can be formulated from phenomenological or mechanistic points of  
66 views. The lack of consensus about the origin of the degradation mechanism  
67 on one hand, and the difficulty of measuring the advance of the reaction  
68 rather than its consequences on the other hand make the formulation of  
69 experimentally based mechanistic models arduous. Nevertheless, there are  
70 some publications which relate macroscopic consequences to a measure of the  
71 reaction. Garcia and colleagues studied the evolution of the pore volume inside  
72 aggregates[12],and measured the evolution of the proportion of the various  
73 types of silica tetrahedra during the swelling. They propose a mechanism  
74 based on a diffuse reaction in the aggregates causing micro-cracking, and note  
75 that the relation between expansion and reaction is strongly influenced by the  
76 degradation state of the aggregates and paste. Ben Haha and colleagues linked  
77 the fraction of the aggregates which reacted to form ASR gel to macroscopic  
78 free expansion.[3].

79 Whether the models be analytical, semi-empirical or numeric, they rely on  
80 underlying hypotheses about the degradation mechanism. The manifestation  
81 of the reaction has been shown by Ponce and colleagues to depend on the

82 mineralogical nature of the aggregates[13]. Aggregates such as opal or vitreous  
83 volcanic rocks react from the surface, with a predominance of gel formation at  
84 the paste-aggregate interface. Mixed mineralogy aggregates, which are more  
85 common in the field, have reactive sites dispersed throughout their volume.  
86 A numerical framework capable of integrating the various microstructural  
87 manifestations of the reaction is therefore necessary to model ASR in general.

### 88 **3 Experimental observations**

89 Ben Haha monitored the expansion of concrete and mortars cast with  
90 moderately reactive aggregates at different temperatures and alkali levels[3].  
91 This experimental study was extended by the current authors with different  
92 aggregates with more varied mineralogies. Polished sections were prepared  
93 for back-scattered electron microscopy observations at intervals.

94 The damage state of the aggregates was measured using the image analysis  
95 methodology developed by Ben Haha and co-workers on the images of the  
96 polished sections. The aggregates were first extracted from the image, then  
97 a threshold was applied to determine the area of voids and cracks in each  
98 aggregate. The ratio of aggregate surface to void surface was used as a direct  
99 measure of the reaction progress (Fig. 2).

100 Ben Haha and colleagues had found a unique relation between expansion  
101 and reacted fraction. They derived a renormalisation function taking into  
102 account the aggregate fraction which allowed the comparison across samples  
103 with varying grain size distributions (Fig. 1). We confirmed this relationship

104 with the new aggregates.

105 The reacted zones were found to be distributed throughout the aggregates.  
106 Similar observations were made on both concrete and mortar samples. This  
107 is consistent with what is reported in the work of Ponce and colleagues for  
108 mixed mineralogy aggregates[13]. These experimental observations served as  
109 a basis for the numerical model with the expansion of randomly distributed  
110 reactive zones randomly in the aggregates, inducing macroscopic expansion  
111 and damage.

## 112 4 Model

113 The microstructural model present here is based on the AMIE framework,  
114 which integrates a set of tools to provide the necessary components for the  
115 simulation of concrete at the microscale: geometry library, mesher, finite and  
116 extended finite element libraries[14], solvers, post-processors. It is optimised  
117 to integrate a number of enrichment sources much larger than that common  
118 in other available software[15, 1].

119 For the simulation of ASR, a typical simulation is as follows. From a  
120 particle size distribution, aggregates are generated and placed in a sample.  
121 In each aggregate reactive zones are generated and placed. The framework  
122 then generates the discrete representation of the setup (Fig. 3). At each step,  
123 boundary conditions are applied, and the reactive zones are caused to expand.  
124 The damage caused by this expansion is computed, and the macroscopic  
125 properties are extracted. The process then repeats a specified number of



126 steps.

127 To investigate in detail the effects of ASR at the meso-scale, an explicit  
128 numerical representation of many factors is required. This implies large  
129 simulations, namely a finely meshed standard mortar bar cross-section of 40  
130 mm  $\times$  40 mm. Such large simulations are necessary as crack-paths within  
131 aggregates spanning the entire particle size distribution will be produced;  
132 direct comparison of the simulations with experimental data is direct and  
133 furthermore features such as the wall effect at mould surface are also simulated.

134 Spherical aggregates are used for simplicity. Indeed, the PSD is known to  
135 affect the reaction, whereas no particular effect of shape has been identified.  
136 Also, the aggregate shape will have little effect because the reactive zones  
137 grow inside the aggregates. The microstructure is generated using a random  
138 packing algorithm, which allows a packing density of 63% of volume with  
139 aggregates to be achieved in a few seconds. The particle size distributions  
140 of the aggregates is taken from that of the real mortars and corrected for  
141 the three dimension to two dimension slicing effect. The ratio of largest to  
142 smallest aggregate is 50, which is a cut off at 200  $\mu\text{m}$ .

143 The reactive zones are explicitly positioned within the aggregates. As  
144 these reactive zones are much smaller than the aggregates and growing as the  
145 reaction proceeds, meshing them would yield problems too large to solve in  
146 reasonable time. Therefore an XFEM representation for the growing reactive  
147 zones was chosen to allow their explicit representation, position, size and  
148 evolution. Although the framework is constructed to allow simulation in  
149 three dimensions it is not practical at present to manage the large amount of

150 data required for such simulations at this resolution, therefore the current  
151 approach is restricted to two dimensions.

152 The mechanical properties of paste and aggregates (stiffness, critical stress)  
153 were obtained experimentally. The simulation of the intrinsic variability of  
154 the paste and aggregates is important to stabilise crack propagation, as  
155 well simulate crack initiation at local defects. Aggregates in ASR-affected  
156 structures exhibit variable mineralogies and so their mechanical properties  
157 will vary at the local level.

158 The influence of the varied nature of the aggregate is simulated by varying  
159 randomly the distribution of the mechanical properties of the elements making  
160 up the aggregates. This local variability is modeled by having the mechanical  
properties  $\mathcal{P}$  of the elements follow a simple statistical law:

$$161 \quad \mathcal{P} = \mathcal{P}_{\text{Prescribed}} \cdot (1 - \xi) + \mathcal{P}_{\text{Prescribed}} \cdot \xi \cdot \omega \quad (1)$$

162 In this equation,  $\omega$  is a random Weibull variable and the the randomised  
163 fraction of the property,  $\xi$ , is set at 0.2; this fraction follows a Weibull law of  
164 mode  $\mathcal{P}_{\text{Prescribed}}$ . This factor was set to reproduce the experimental spread  
165 observed in mechanical tests.

166 The paste fills the space not occupied by the aggregates and has similarly  
167 randomised properties. Both aggregates and paste are assumed to be linear  
168 elastic, with damage. The finite element formulation for linear elasticity is

implemented using the usual form (Eq. 2).

$$\mathbf{K}_{ij}^e = \int_e \nabla h_i \mathbf{E}^e \nabla h_j \, de \quad (2)$$

In this equation  $e$  marks the element contribution,  $h_i$  is the  $i^{\text{th}}$  shape function,  $\mathbf{K}_{ij}^e$  the elementary contribution to the global stiffness matrix, for the  $i^{\text{th}}$  and  $j^{\text{th}}$  shape functions,  $\mathbf{E}^e$  the element's Cauchy-Green stress tensor. The per-shape function formulation makes this formulation equally valid for extended finite elements.

Once the microstructure has been generated, it is meshed conformantly using a Delaunay mesher, developed in-house around the core meshing algorithm from Devillier and colleagues [16]. The samples were finely meshed to capture the fracture pattern within the aggregates and the paste.

## 4.1 Damage Model

Damage at the meso-scale is induced by a dense network of cracks. Because of the multiplicity of those cracks, special care must be taken that their propagation corresponds to a global energy minimum. The algorithm outlined in Fig. 4 ensures this is the case, even if multiple fracture criteria and damage mechanisms coexist. This approach leads to simulated fracture patterns which are qualitatively similar to the experimentally observed ones (Fig. 5).

Also, the more usual method of iterating on the load state to match the damage is not applicable, as the damage is induced by a load prescribed by

188 the setup of the simulation. Thus, the fracture propagation to the point of  
189 equilibrium must be determined *a posteriori*, after the load has been set.

190 As both paste and aggregates can be considered quasi-brittle, we have  
191 opted for the following damage evolution law where the damage evolution  
192 parameter  $\eta$  is adjusted to the experimentally measured material parameters  
and  $\varepsilon$  is an arbitrarily small value.

$$193 \quad d^{i+1} = \max(d^i + e^{\eta d^i}, 1 - \varepsilon) \quad (3)$$

194 Where  $d$  is a factor such that the Young's modulus  $E$  is related to the original  
modulus by the equation 4.

$$195 \quad E = (1 - d)E_0 \quad (4)$$

196 The damage is incremented when a failure criterion is reached. The failure  
197 criterion used in our simulations is a modified Mohr-Coulomb criterion. It  
198 is reached when the maximum principal stress is beyond a critical value in  
199 tension or compression.

200 To ensure that the damage is applied on a non-local basis, a neighbourhood  
201 is defined for each element which defines the density of elements which can  
202 be damaged at each step of the damage computation. A neighbourhood of  
203 the size of the average inter-aggregate distance yielded results closest to the  
204 experiments. To determine which elements should be damaged at each step of  
205 the damage computation loop, we defined a score which allows inter-element

206 comparison. This score is based on the distance to the fracture surface defined  
207 by the criterion. In those simulations, the score  $s$  is calculated as defined in  
equation 5.

$$208 \quad s = 1 - \frac{\sigma_{\max}}{\sigma_{\text{crit}}} \quad (5)$$

## 209 4.2 Gel Model

210 Microscopic observation of a wide range of mineralogically different aggre-  
211 gates consistently revealed the presence of ASR gel pockets in the aggregate.

212 The originality of our model lies in the fact that the gel pockets are  
213 explicitly considered, so the damage in the aggregates and paste emerges  
214 from the numerical setup of the meso-structure directly. The implementation  
215 of this feature required the use of modern developments in both numerical  
216 theory and numerical methods.

217 Gel pockets are modelled using a soft-discontinuity type of enrichment.  
218 This type of enrichment simulates a perfect contact between two materials  
219 of distinct mechanical properties. The enrichment function  $\phi$  used was  
introduced by Moës and colleagues[15].

$$220 \quad \phi(\mathbf{x}) = 1 - \frac{|\mathbf{x} - \text{proj}_{\Gamma_{\text{gel}}} \mathbf{x}|}{\Gamma_{\text{gel}}} \quad (6)$$

221 With  $\Gamma_{\text{gel}}$  the gel boundary,  $\text{proj}$  the projection operator, and  $\mathbf{x}$  coordinates  
222 in the global system.

223 The integration step is performed by generating a temporary conformant  
224 tessellation of each enriched element. The generated mesh is then refined until  
225 convergence of the domain integral of the enrichment functions is reached.  
226 The final quadrature generated in this way is then used for the integration of  
227 the weak form defining the behaviour, and the temporary mesh is discarded  
228 (Fig. 6).

229 Using this approach, we can model the gel by taking into account the  
230 spatial distribution of the reactive zones, their size and the interface between  
231 the gel and the aggregates. The gel properties are assumed to be linear elastic  
232 with an imposed strain, as the gel is constrained by its surroundings until  
233 large amounts of damage have occurred. Using XFEM, we can accurately  
234 represent the geometry in each simulation step as illustrated on Fig. 7.

235 The gel mechanical properties are not well known, and experimental  
236 measures exhibit important variability in terms of the chemical nature of  
237 the gel[17] and its apparent mechanical properties[18, 19, 20]. However, the  
238 chemistry of the ASR gel, is close to that of C-S-H. For this reason, we have  
239 decided to assume that the gel is quasi-incompressible, with a Poisson ratio of  
240 0.49997, that of water, and a stiffness which is a fraction of that of C-S-H[21],  
241 expressed in the figures as  $\alpha$ .

242 The free expansion of the gel is, like the mechanical properties, difficult to  
243 measure experimentally. However, it can be obtained by fitting the early part  
244 of the free expansion-damage curve. In the very early stages of the reaction,  
245 the damage from induced cracks is very little, and the expansion of the sample  
246 can be assumed to be elastic. From this we can obtain the expansive property

247 of the gel which would result in this expansion. We found that a 50% volume  
 248 expansion fits the experiments. The variability of the image analysis method  
 249 at the early age of the reaction makes it difficult to be very precise about this  
 250 value. However, the overall result of the simulation is not very sensitive to  
 251 the value taken and 50% is also consistent with the stoichiometric volumetric  
 252 ratio reported by Garcia and colleagues [12].

253 The strain of the gel,  $\varepsilon_{\text{imp}}$  is imposed as a virtual force on the nodes of the  
 254 elements inside or cut by the gel pockets. The integration scheme is generated  
 255 such that only the fraction of the element where the swelling takes place is  
 accounted for (Eq. 7).

$$256 \quad \mathbf{f}_i = \int_{\Omega_{\text{gel}} \cap e} \nabla h_i \mathbf{E} \varepsilon_{\text{imp}} \, d(\Omega_{\text{gel}} \cap e) \quad (7)$$

257  $\Omega_{\text{gel}}$ , the gel surface,  $e$  the element surface,  $h_i$  the shape function associated to  
 258 the degree of freedom considered,  $\mathbf{f}_i$  the associated force,  $\mathbf{E}$ , the Cauchy-Green  
 259 stress tensor of the gel.

### 260 4.3 Reaction Mechanism Model

261 The model presented here is at present achronic. The sample expansion is  
 262 computed only against the degree of reaction, which is the part of aggregate  
 263 which has reacted to form ASR gel. Thus the mechanical model cannot yet  
 264 take into account such time-dependent behaviour as gel flow and paste creep  
 265 depending on the curing conditions. As reaction could take weeks or years,  
 266 creep may be important and we expect our model to predict expansions higher

267 than the experimentally measured ones at the later stages of the reaction, as  
268 no relaxation mechanism is present other than cracking.

269 The gel is grown by steps in each aggregate until a preset percentage (3%)  
270 of the considered aggregate has reacted, at which point we stop the reaction  
271 in that aggregate. To verify the influence of gel growth capping per particle,  
272 we ran simulations where all gel pockets grow in the same way, independent  
273 of their location. The gel is principally located in the larger aggregates, as  
274 they form the main fraction of aggregate volume. Thus, stopping the reaction  
275 in the smaller aggregates has little effect on the final expansion. However,  
276 the initial shape of the expansion-reaction curve is slightly affected.

277 By the end of the run nearly half of all aggregates have exhausted their  
278 expansion potential (Fig. 8). This effect can be simulated explicitly in our  
279 model as the full PSD is represented.

## 280 **5 Results**

### 281 **5.1 Simulation of the Free Expansion of Mortars**

282 The simulated expansion-reaction curves follow the early part of the  
283 experimental dataset, but reach a plateau at higher expansions. The jitters  
284 observed in the simulated curves start at the onset of paste failure, which  
285 happens at the same reaction level as in the experiments. The higher final  
286 expansion can be explained by the absence of strain relaxation mechanisms  
287 in the paste other than crack propagation: there is no creep (Fig. 9).



288 As shown in Fig. 10, the measured damage and the actual reaction diverge.  
289 For this reason we have only simulated expansions up to 1% of reaction. At  
290 this level significant damage has occurred (Fig. 11), beyond what would have  
291 been considered critical in a structure.

292 The expansion-reaction curves obtained from simulation match the exper-  
293 iment well within the observed variability, with no fitting parameters other  
294 than the stiffness and free expansion of the gel. We found that the range  
295 of gel stiffness which could fit the experimental relationship is quite large:  
296 between 0.6 and 0.9 of that of C-S-H.

## 297 **5.2 Prediction of the loss of mechanical properties**

298 From the average stress and strain of the samples at each time point,  
299 we can compute the apparent stiffness of the sample, and thus link the  
300 advancement of the reaction to the damage level in the sample. These results  
301 are then compared to experimental values reported in the literature (Fig. 11).

302 The loss in stiffness is mostly due to the aggregates cracking, as the paste  
303 is mostly in compression, with stress levels below the elastic limit. Paste  
304 failure occurs only when cracks from the aggregates reach the paste, thus  
305 increasing the tensile stress locally and initiating failure there. This also  
306 means that the properties of the interfacial transition zone between paste  
307 and aggregate, which we have not at present included in our model will have  
308 negligible impact on the damage evolution.

309 The loss of stiffness predicted by the simulation is consistent with data

310 reported in the thesis of Ben Haha[22], but is sensitive to the choice of gel  
311 properties at low reaction values.

### 312 **5.3 Sensitivity to the Various Parameters**

313 Several simulation campaigns were run to verify that our results are not  
314 sensitive to numerical effects. First we verified sensitivity to mesh size. The  
315 characteristic element size was halved, yielding four times as many elements,  
316 and the same simulation was run. The results are not significantly different  
317 when using a much finer mesh. This verifies both the XFEM model for the  
318 expansive zones and the energy-conservation of the damage model. The  
319 expansion values vary by only 2% at the final degree of reaction (e.g. at 1%  
320 expansion, the error is  $\pm 0.02\%$ ).

321 Another second simulation campaign was run with a microstructure as  
322 dense as the packing algorithm allows. A mortar sample was generated with  
323 a packing density of 71%, larger than the value from the experimental mix  
324 design. The final expansions differed by only a relative amount of 6%, which  
325 is consistent with the increase in reactive material.

326 Finally we also verified the sensitivity to the variability of the local  
327 mechanical properties. We varied from 0.2 to 0.5 the weight  $\omega$  (See Eq. 1).  
328 Increase in variability lead to earlier cracking, but does not affect measurably  
329 the results.

## 330 **6 Discussion**

### 331 **6.1 Correlation Between Damage and Reaction**

332 Image analysis cannot distinguish well between reaction (gel or voids)  
333 and damage (cracks): both appear as dark zones in the aggregate. In our  
334 simulations we compared the apparent reaction, as would be measured by  
335 the image analysis and the effective reaction, which is given as an input in  
336 the program. As expected, the apparent damage is larger than the effective  
337 reaction percentage. However they are close, and quasi-linearly related, if  
338 divergent. The cracks do not represent a significantly large volume of damage,  
339 compared to the volume of the gel pockets (Fig. 10).

340 The apparent expansion-reaction curve is less sensitive to the fit parameters  
341 than the real one (Fig. 12). This is explained by the strong link between  
342 damage and expansion, which is more direct than the link between expansion  
343 and reaction. This further explains the low variation observed experimentally  
344 across aggregate types and curing conditions. The noise apparent in the  
345 simulated damage-expansion curve is due to the healing effect of gel growing  
346 over fractured aggregate matter. This variation is consistent with experimental  
347 variability.

### 348 **6.2 Expansion Mechanism**

349 The expansion-reaction curve exhibits three regimes: Linear expansion,  
350 aggregate cracking and paste cracking (Fig. 13). The simulation shows that

351 this is the result of four mechanisms: the expansion caused by the gel, the  
352 relaxation from the damage, the interaction between the gel zones, and the  
353 creep. The growth of the reactive zones can be measured as the reaction  
354 advances, and provides an insight into the expansion mechanism. In the first  
355 stage, as the gel progressively damages the aggregates, the expansion becomes  
356 less and less restrained until a plateau is reached, at this point the gel is  
357 essentially free to expand in the aggregates. This plateau comes to an end  
358 as the paste starts restraining further expansion. This evolution is mostly  
359 governed by the evolution of damage, and is not very sensitive to the gel  
360 stiffness parameter, but rather to gel localisation. It should be noted that  
361 the expansions at the end of the first stage are already well in excess of those  
362 likely to cause structural problems in large unreinforced structures such as  
363 dams.

364 As expected, the simulated expansion levels off at a higher point than the  
365 experimental ones (Fig. 12). This can be explained by the time-dependent  
366 visco-elastic behaviour of the gel and the creep of the paste not being modelled  
367 in these simulations, which leads to less strain relaxation than in real samples.

### 368 **6.3 Comparison to Simpler Models**

369 Various simplifications have been proposed for meso-scale modelling of  
370 ASR (Fig. 14). The simplest model applies a pseudo-thermal expansion for  
371 the aggregates as a source for the expansion. We found it possible to calibrate  
372 such model to fit the early part of the curve, using a linear correlation between  
373 the imposed strain and the degree of reaction. However, such a model does not

374 capture the damage in the aggregates, and thus the loss in physical properties  
375 (Fig. 15).

376 The predictive nature of such a model is low, as the expansion of the  
377 aggregate must be computed as an empirical function of the degree of reaction.  
378 Such models have been used in the past to predict free expansion, using  
379 reduced particle size distributions. However the simulations demonstrates  
380 that such models are extremely dependent on the PSD of the aggregates,  
381 and exhibit very different damage patterns depending on the accuracy of  
382 the representation of the microstructure. Simplification of the PSD has  
383 consequences on the evolution of damage. A dense packing of aggregates  
384 causes all the paste to be in compression, whereas a reduced packing allows  
385 for higher shear levels in the paste, which then leads to cracking at lower  
386 levels of macroscopic expansion in those simulations.

387 When the local stress around the aggregates reaches a critical threshold,  
388 the sample undergoes critical failure. We found the critical failure to occur  
389 at the same imposed expansion, independently of the aggregate content.

390 The expansion-reaction curve observed experimentally exhibits different  
391 regimes: linear expansion, aggregate failure, paste failure(Fig. 13). The  
392 simplified model can capture the first and last regimes. When the local stress  
393 around the aggregates reaches a critical threshold, the sample undergoes  
394 catastrophic failure. The stress imposed by the aggregates needs to be fit  
395 with an empirical model which would include the effect of the damage in the  
396 aggregates. As such, this simplified model is incomplete if using only directly  
397 measured experimental values.

398 Another simple model for the reaction which has been proposed is that the  
399 gel is formed as a rim around the aggregate. Such a microstructural makeup  
400 has never been explicitly simulated, but this vision of the reaction is used  
401 as the source of other semi-empirical models, such as the growing aggregate  
402 model described above. This model can be correlated to an advance of the  
403 reaction, as the gel localisation and amount are explicitly defined for each step  
404 of the reaction. To test this model, we implemented an enrichment scheme  
405 which could reproduce the two distinct interfaces between the aggregate and  
406 the gel, and between the gel and the paste.

407 This model is different from the precedent in that it explicitly affects the  
408 bond properties between aggregates and paste.

409 The fracture patterns obtained in such a setup show this model is not  
410 a good candidate to explain the ASR degradation: The cracks are located  
411 in the paste, while the aggregates remain largely intact, except for cracks  
412 initiating at the interface. Considerable decohesion between the aggregates  
413 and the paste is also observed (Fig. 16).

414 The simulations show that the macroscopic expansion and damage are  
415 strongly linked to the microstructural localisation of the reaction. Thus, the  
416 prediction of expansion from the advance of the reaction is only possible in  
417 models which simulated the direct consequences of ASR at the microstructure  
418 level.

## 419 **7 Conclusion and perspectives**

420 This paper presents a physically-based model of ASR, implemented and  
421 tested in a custom-developed FE framework. The model highlights the pre-  
422 dominant effect of gel formation in the aggregates in the ASR degradation  
423 mechanism, notably damage in the aggregates themselves. The loss of me-  
424 chanical properties can be wholly explained by the damage induced by the gel,  
425 and the model can be used to predict the evolution of mechanical properties.  
426 The model presented here showed robustness to the variation of the single fit  
427 parameter, apparent gel stiffness.

428 The implementation of simplified models commonly used to explain the  
429 mechanical effects of the reaction shows them to be inadequate to capture the  
430 physics of the phenomenon. The usual simplifications entail the transfer of  
431 the damage from the aggregates to the cement paste, which is experimentally  
432 observed to occur only during the advanced stages of the reaction. We also  
433 find that the shape of the free expansion/reaction curve cannot be captured  
434 by these models, unless it is imposed.

435 These simulations demonstrate the capacity of our finite element frame-  
436 work to perform well with an extremely high density of enrichments, which  
437 illustrates the robustness of our implementation.

438 Future work involves coupling the model with a diffusion mechanism for  
439 the alkali ions, and the introduction of time-dependent creep, which would  
440 serve as a base for a kinetic simulation of ASR.

## 441 8 Acknowledgments

442 We would like to thank the Swiss Federal Office of Energy for their support,  
443 financial or otherwise.

## 444 References

- 445 [1] C. Dunant, P. N. Vinh, M. Belgasmia, S. Bordas, and A. Guidoum,  
446 “Architecture tradeoffs of integrating a mesh generator to partition of  
447 unity enriched object-oriented finite element software,” *Revue européenne*  
448 *de mécanique numérique*, vol. 16, pp. 237–258, 3 2007.
- 449 [2] S. Bordas, V. P. Nguyen, C. Dunant, H. Nguyen-Dang, and A. Guidoum,  
450 “An extended finite element library,” *International Journal for Numerical*  
451 *Methods in Engineering*, vol. 71, pp. 703–732, 1 2007.
- 452 [3] M. ben Haha, E. Gallucci, A. Guidoum, and K. L. Scrivener, “Relation of  
453 expansion due to alkali silica reaction to the degree of reaction measured  
454 by sem image analysis,” *Cement and Concrete Research*, vol. 37, pp. 1206–  
455 1214, 8 2007.
- 456 [4] B. Capra and J.-P. Bournazel, “Modeling of induced mechanical effects  
457 of alkali-aggregate reactions,” *Cement and Concrete Research*, vol. 28,  
458 no. 2, pp. 251–260, 1998.
- 459 [5] S. Poyet, *Etude de la dégradation des ouvrages en béton atteints par la*  
460 *réaction alcali-silice : Approche expérimentale et modélisation numérique*



- 461 *multi-échelles des dégradations dans un environnement hydro-chemo-*  
462 *mécanique variable.* PhD thesis, Université de Marne-La-Vallée, 2003.
- 463 [6] E. M. R. Fairbairn, F. L. B. Ribeiro, L. E. Lopes, R. D. Toledo-Filho,  
464 and M. M. Silvano, “Modelling the structural behaviour of a dam affected  
465 by alkali–silica reaction,” *Commun. Numer. Meth. Engng*, pp. 1–12, 7  
466 2005.
- 467 [7] S. Multon and F. Toutlemonde, “Effect of applied stresses on alkali–silica  
468 reaction-induced expansions,” *Cement and Concrete Research*, no. 36,  
469 pp. 912–920, 2006.
- 470 [8] C. Larive, *Moyens et Méthodes d’Essai. études et recherches des labora-*  
471 *toires des ponts et chaussées ed.*, 1998.
- 472 [9] T. Ichikawa and M. Miura, “Modified model of alkali-silica reaction,”  
473 *Cement and Concrete Research*, pp. 1291–1297, 6 2007.
- 474 [10] Z. P. Bažant and A. Steffens, “Mathematical model for kinetics of alkali-  
475 silica reaction in concrete,” *Cement and Concrete Research*, pp. 419–428,  
476 12 1999.
- 477 [11] O. Çopuroğlu and E. Schlangen, “Modelling of effect of asr on concrete  
478 microstructure,” *Key Engineering Materials*, vol. 348, pp. 809–812, 09  
479 2007.
- 480 [12] E. Garcia-Diaz, J. Riche, D. Bulteel, and C. Vernet, “Mechanism of  
481 damage for the alkali–silica reaction,” *Cement and Concrete Research*,  
482 pp. 395–400, 6 2006.

- 483 [13] J. Ponce and O. Batic, “Different manifestations of the alkali-silica  
484 reaction in concrete according to the reaction kinetics of the reactive  
485 aggregate,” *Cement and Concrete Research*, no. 36, pp. 1148–1156, 2006.
- 486 [14] I. Babuška and I. Melenk, “Partition of unity method,” *International  
487 Journal for Numerical Methods in Engineering*, vol. 40, no. 4, pp. 727–758,  
488 1997.
- 489 [15] N. Moës, M. Cloirec, P. Cartraud, and J. Remacle, “A computational  
490 approach to handle complex microstructure geometries,” *Comput. Meth.  
491 Appl. Mech. Eng.*, vol. 192, no. 29, pp. 3163–3177, 2003.
- 492 [16] O. Devillers, S. Meiser, and M. Teillaud, “Fully dynamic delaunay trian-  
493 gulation in logarithmic expected time per operation,” *Comput. Geom.  
494 Theory Appl.*, vol. 2, no. 2, pp. 55–80, 1992.
- 495 [17] C. Tambelli, J. Schneider, N. Hasparyk, and P. J. Monteiro, “Study of the  
496 structure of alkali-silica reaction gel by high-resolution nmr spectroscopy,”  
497 *Journal of Non-Crystalline Solids*, pp. 3429–3436, 8 2006.
- 498 [18] A. Binal, “The determination of gel swelling pressure of reactive aggre-  
499 gates by asgpm device and a new reactive-innocuous aggregate decision  
500 chart,” *Constr Build Mater*, vol. 22, pp. 1 – 13, 1 2008.
- 501 [19] J. E. Dolbow, E. Fried, and H. Ji, “Chemically induced swelling of  
502 hydrogels,” *Mechanics and Physics of Solids*, 2003. in press.

- 503 [20] M. Kawamura and K. Iwahori, “Asr gel composition and expansive  
504 pressure in mortars under restraint,” *Cement & Concrete Composites*,  
505 no. 26, pp. 47 – 56, 2004.
- 506 [21] G. Constantinides and F.-J. Ulm, “The effect of two types of c-s-h term  
507 on the elasticity of cement-based materials: Results from nanoindentation  
508 and micromechanical modeling,” *Cement and Concrete Research*, no. 34,  
509 pp. 67–80, 2004.
- 510 [22] M. ben Haha, *Mechanical Effects of Alkali Silica Reaction in concrete*  
511 *studied by SEM-image analysis*. PhD thesis, EPFL, 5 2006.

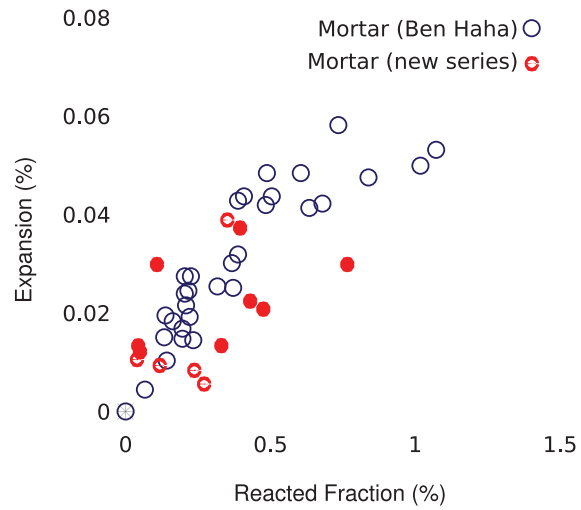


**Figure 1:** Experimental relationship between measured free expansion and measured reacted fraction. Results from Ben Haha [3], as well as from the current study are reported.

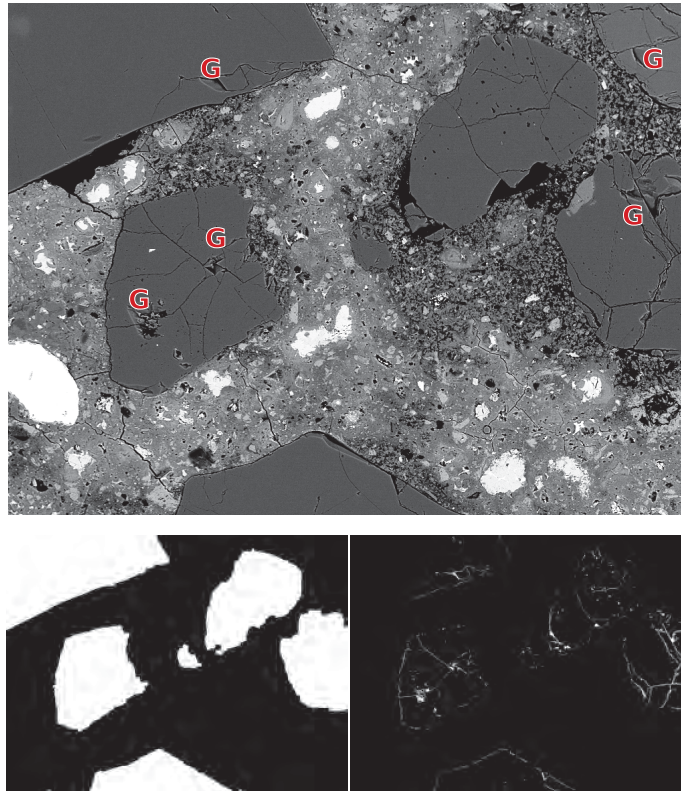


**Figure 2:** Image analysis procedure used to extract the degree of reaction. The aggregates are extracted from the original image (top) as a mask (bottom left), and the damage in the aggregates is obtained through thresholding (bottom right). Gel packets are marked with **G**.

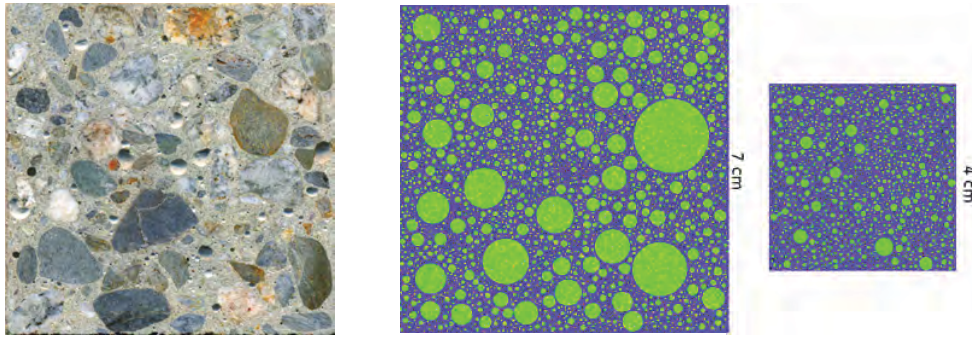


**Figure 3:** Simulated concrete (centre) and mortar microstructures (right), compared to an actual slice (left)

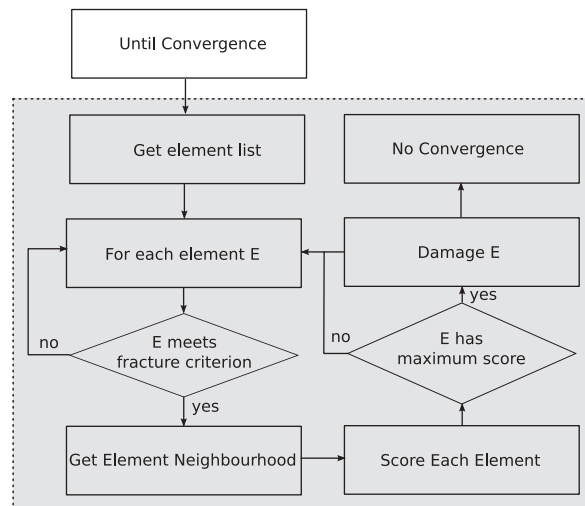


**Figure 4:** Flow diagram of the algorithm which determines which element must be damaged. This method ensures that at each step of the cracking process the damage increment minimises the global energy. If the increment is small enough, this method effectively reproduces the damage history which corresponds to the global energy minimum.

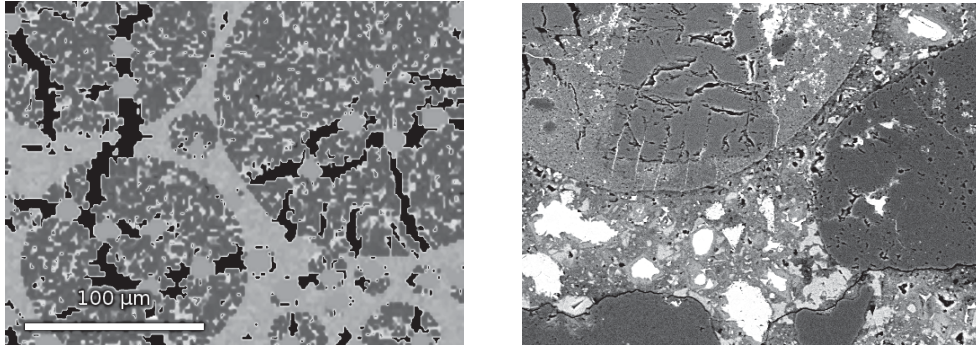


**Figure 5:** Detail of a fracture pattern generated by the ASR model (left). For comparison, a micrograph at the same scale of an aggregate (right).

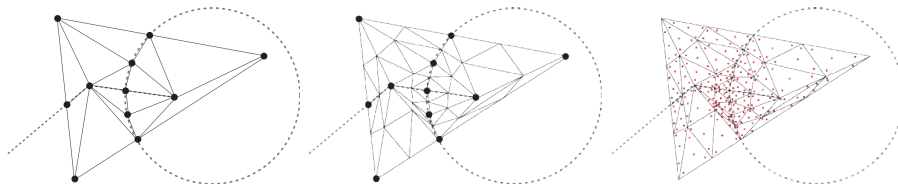


**Figure 6:** Steps in the generation of a quadrature. A conformant mesh is generated as a function of the geometrical base of the enrichments. This mesh is refined using an adaptive quad-tree algorithm. The Gauß points are kept, and the sub-mesh discarded.

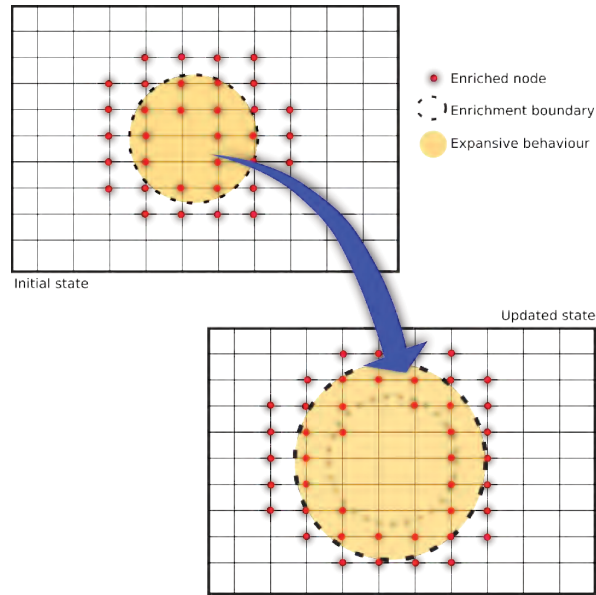


**Figure 7:** Update of the enrichment scheme. The scheme is illustrated on a structured rectangular mesh for clarity, however, the mesh used in the simulations are triangular unstructured.

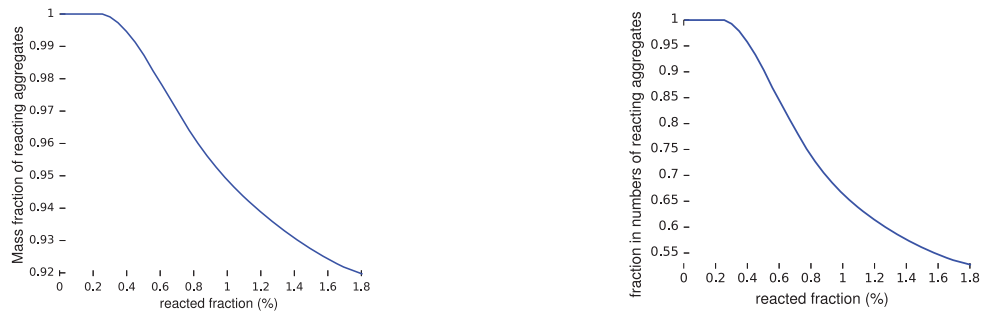


**Figure 8:** Fraction of the mass of individual aggregates where the reaction has been stopped as a function of reaction advancement (left). Fraction of the number of individual aggregates where the reaction has been stopped as a function of reaction advancement (right).



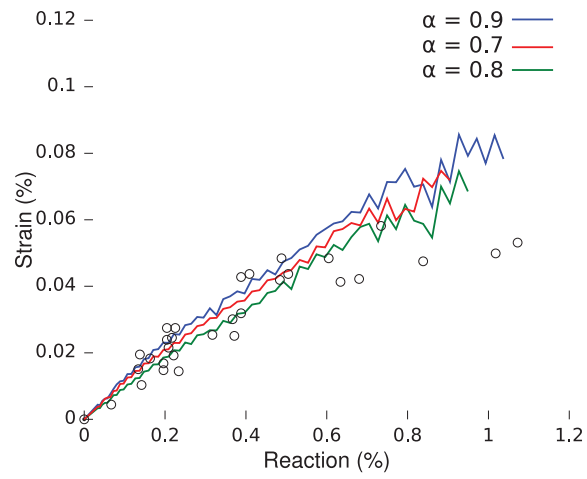


**Figure 9:** Simulated expansion-reaction curve for mortar. The curves are not prolonged because a state is reached where the samples are not of a single piece anymore.

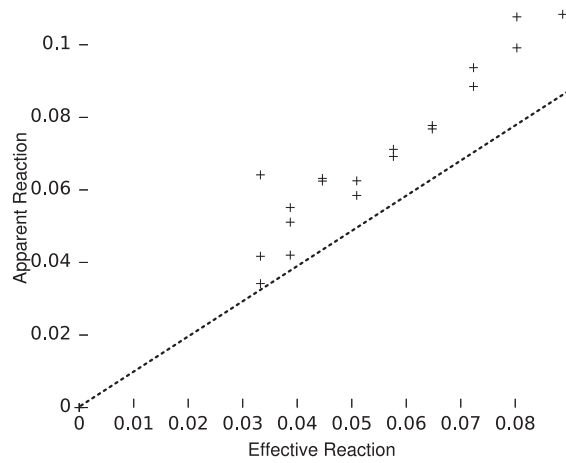


**Figure 10:** Apparent reaction as a function of effective reaction. The dotted line is the line of equality.

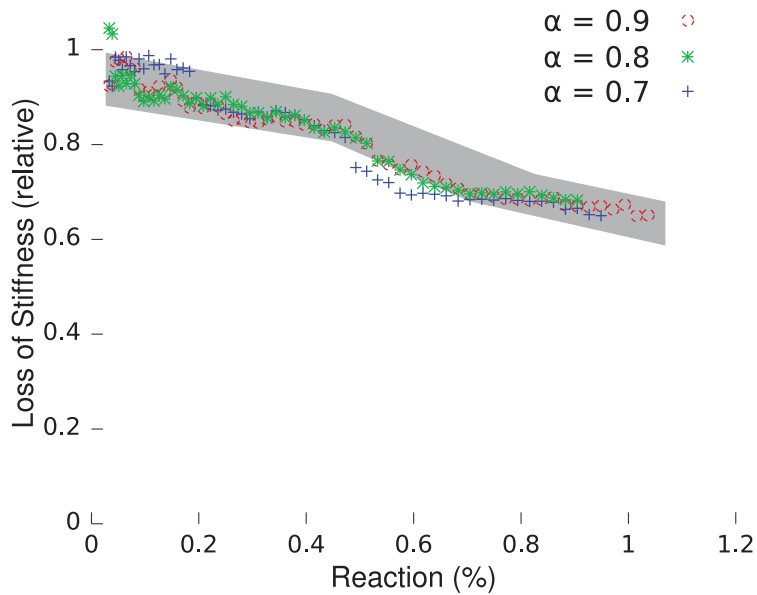


**Figure 11:** Stiffness as a function of the progress of the reaction(left). The loss of stiffness as a function of expansion is compared tot a range of reported values from Ben Haha (grey shade).

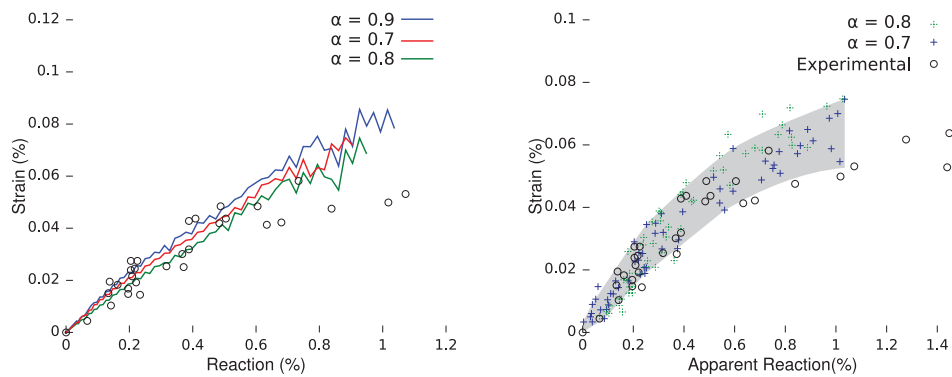


**Figure 12:** Comparison between the real expansion-reaction curve (left) and the apparent one (right). The point where the expansions reach a plateau is higher than the experimentally measured values in both cases. This indicates that a relaxation mechanism is not taken into account in the simulations.

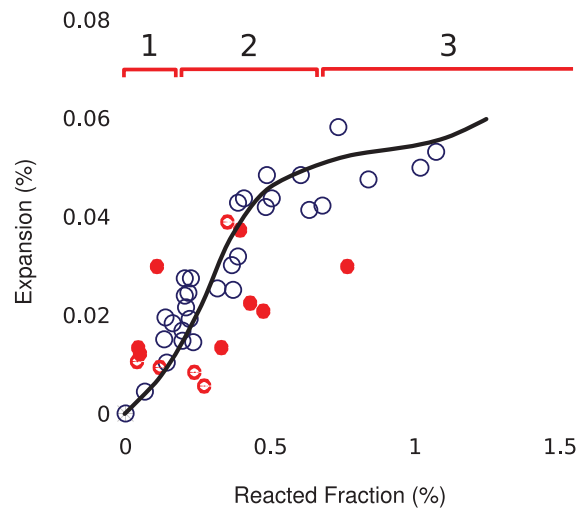


**Figure 13:** Mechanism for expansion and degradation. (1) Elastic expansion; (2) Aggregate failure and gel pressure buildup; (3) Paste cracking.

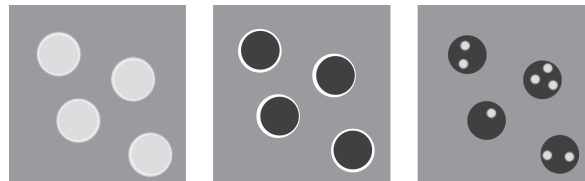


**Figure 14:** Three Models for ASR-induced expansion. Homogenised aggregate expansion (left), gel rim expansion (centre), gel pockets expansion (right).

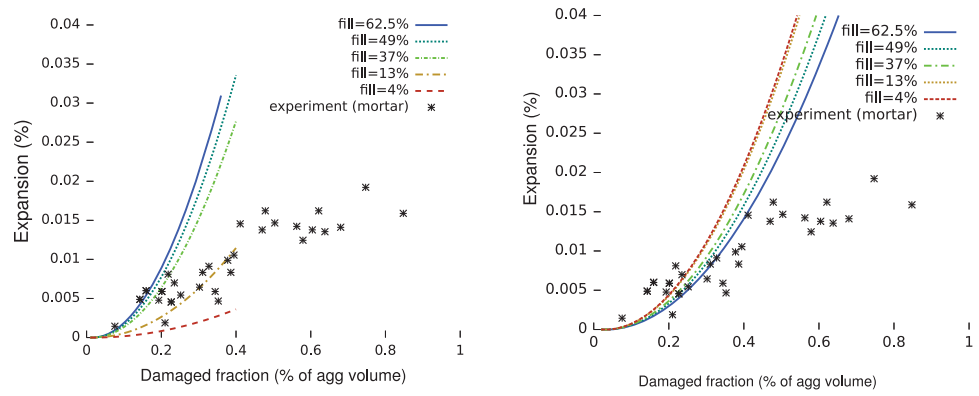


**Figure 15:** Expansions predicted by a simplistic model, with varying cutoff points in the PSD (left). Expansions have been renormalised according to the aggregates content (right).

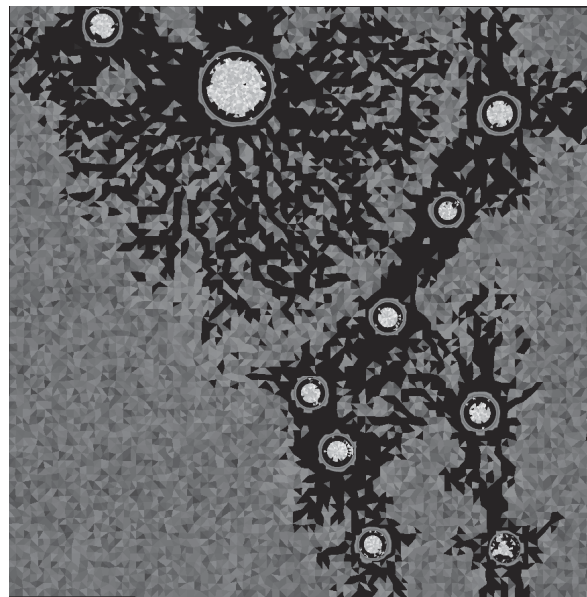


**Figure 16:** Crack patterns produced by an expansive ring of gel formed around the aggregates.